We are IntechOpen, the world's leading publisher of Open Access books Built by scientists, for scientists

4,800
Open access books available

122,000
International authors and editors

135M
Downloads

Our authors are among the

154
Countries delivered to

TOP 1%
most cited scientists

12.2%
Contributors from top 500 universities

CLARIVATE ANALYTICS BOOK CITATION INDEX INDEXED

WEB OF SCIENCE™

Selection of our books indexed in the Book Citation Index in Web of Science™ Core Collection (BKCI)

Interested in publishing with us?
Contact book.department@intechopen.com

Numbers displayed above are based on latest data collected.
For more information visit www.intechopen.com

2

Spectroscopic and Dielectric Characterization of Plasma Sprayed Titanates

Pavel Ctibor[1] and Josef Sedlacek[2]
[1]*Institute of Plasma Physics, ASCR, v.v.i., Prague,*
[2]*Department of Electrotechnology, Faculty of Electrical Engineering,*
Czech Technical University, Prague
Czech Republic

1. Introduction

Synthetic perovskite $CaTiO_3$ (CT), geikielite $MgTiO_3$ (MT) and their mixture $MgTiO_3$-$CaTiO_3$ (MCT) are materials well known and widely used as dielectrics in a sintered state. CT is high-permittivity linear dielectric material whose structure is not influenced by plasma spraying - neither chemical nor phase composition, as demonstrated earlier [Ctibor, 2003]. MT belongs to the family of low-loss microwave dielectrics and MT-CT solution is known by its temperature stability of permittivity. Namely the composition $(Mg_{0.95}Ca_{0.05})TiO_3$ is used in connection with this feature.

In recent decades plasma spraying has become a well accepted technology as the coating method for metallic and ceramic materials and has been used in a variety of fields including electrical engineering. The coatings have lamellar character of a body formed with porosity aligned with respect to the lamellas. Spraying does not require heating of the substrate to the melting point of the deposited material.

Often the research is focused on the microstructure of plasma sprayed coatings and features like porosity, unmelted particles, cracks and residual stress. Above listed characteristics are responsible for the behavior of coatings. However in the case of titanates phenomena taking place on atomic level and single crystal cell level are also important. Raman spectroscopy, infrared spectroscopy and near-field microwave microscopy are suitable techniques for this characterization.

Ca and Mg have the same charge but different ionic radii (rCa^{2+} = 0.134 nm and rMg^{2+} = 0.103 nm) [Hirata, 1996]. A mixture of CT and MT melts and forms an eutectic liquid at 1462°C, which, under proper solidification conditions, can be used to achieve a highly dense product. During processing presence of intermediate phases of $MgTi_2O_5$ and Mg_2TiO_4 was noted, and they were difficult to eliminate completely from the reaction products [Zhang, 2006; Zheng, 2003; Huang, 2002].

MCT exhibits differences from MT in the metal-oxygen bond lengths which are relevant to the stability of the compounds. While the infrared and Raman spectra of CT and MT have been measured [Jiang, 1998; Cavalcante, 2008], other cations at the *A* and/or *B* sites alters the vibrational properties of ABO_3 studied by these spectroscopic techniques. This encourages the author to measure the Raman and infrared spectra. In the plasma sprayed MCT we have earlier recognized also $MgTi_2O_5$ and Mg_2TiO_4 phases [Ctibor, 2003].

Besides the mentioned dielectric titanate materials we have sprayed also one representative of ferroelectrics - barium titanate. $BaTiO_3$ (BT) is an interesting multifunctional oxide that exhibits complex phase appearance. Between 120°C (393K) and 1457°C (1730K) $BaTiO_3$ has a cubic perovskite structure that consists of corner linked oxygen octahedra containing Ti^{4+}, with Ba^{2+}. Cooling below 120°C results in small displacements in the positions of the cations in the unit cell resulting in polar ferroelectric phase existing in the temperature interval between 5°C (278K) and 120°C [Boutinaud, 2006].

$BaTiO_3$, due to its high dielectric constant, is used frequently as multilayer capacitor components and sensors. However, it has been found that with respect to the electrical properties $BaTiO_3$ in the form of thin-films does not reach the qualities of bulk material. This difference was explained by a combination of the intrinsic dead layer effect, a stress effect, an effect of the microstructure within the thin film, and an effect of the stoichiometry [Zhao, 2008]. In particular, the relative permittivity of films decreases when the film thickness is reduced [Setter, 2000]. The optimal dielectric characteristics are obtained for sintered $BaTiO_3$-based sample with bulk density of about 5300 $kg.m^{-3}$ [Jin, 2003]. Any deviation from the stoichiometric Ba/Ti ratio leads to suppression of the high relative permittivity of the ferroelectric barium titanate [Mitic, 2001]. To detect the tetragonal $BaTiO_3$ phase by X-ray diffraction, the split of peaks of (002) and (200) reflection is a well-established indication [Waser, 1999; Yu, 2009; Simon-Seveyrat, 2007].

In general there are differences of the behavior of barium titanate in the form of a single-crystal, sintered bulk material and thin film [Boutinaud, 2006; Mitic, 2001]. Plasma spraying enables to create layers with 'bulk-like' thickness but adhering on a metallic substrate of various shapes. Free-standing parts of titanate ceramics can be fabricated as well by plasma spraying [Wu, 2009]. $BaTiO_3$ itself was up to now very seldom plasma sprayed and the understanding of its behavior in the form of sprayed coating is not satisfactory. For coatings with the thickness of about 100 μm the values of relative permittivity 50 and loss factor 0.08 were reported [Dent, 2001]. The dielectric properties of the plasma sprayed $BaTiO_3$ were related to the degree of crystallinity [Dent, 2001]. The coatings containing more crystalline material have higher relative permittivity. The relative permittivity was affected also by cracks and splat interfaces within the coating [Dent, 2001]. The reported value of relative permittivity is however surprisingly low, because one and more orders higher values are typical for bulk $BaTiO_3$ [Buchanan, 2004].

In frame of the presented chapter we are focused on selected aspects of the dielectric characteristics of the as-sprayed barium titanate coatings and we provide comparison of them with other plasma sprayed titanates.

2. Experimental

2.1 Feedstock materials

All materials were obtained in the form of tablets of industrial purity, produced by the sintering of micropowders. The sintering was carried out by companies Epsilon (Librice, Czech Republic), Ceramic Capacitors (Hradec Kralove, Czech Rep.) and Teceram (Hradec Kralove, Czech Rep.).

The synthetic form of perovskite $CaTiO_3$ was produced by reactive sintering of CaO and TiO_2. $CaTiO_3$ powder used for experiments was sintered without any additives (like ZnO), normally used for decreasing the sintering temperature. Tablets were crushed and sieved into a powder of the correct size for spraying. $MgTiO_3$ and MCT were sintered using MgO, $CaCO_3$ and TiO_2. After sieving the size distribution of the feedstocks was 63–125 microns for all three materials.

$BaTiO_3$ feedstock powder was obtained by crushing and sieving of sintered coarse agglomerates. Those agglomerates were prepared by a reactive sintering of micrometer-sized powders of $BaCO_3$ and TiO_2 used as starting materials. After sieving the size distribution of the BT feedstock for spraying was between 20 and 63 μm with an average at 40 μm, whereas the bulk density measured by helium pycnometry was 5721 $kg.m^{-3}$.

2.2 Plasma spraying

The CT, MT and MCT samples were manufactured using a high throughput Water-Stabilized Plasma (WSP) spray system WSP500® at Institute of Plasma Physics (Prague, Czech Republic) at ambient atmosphere. The WSP system operates at about 160 kW arc power and can process high amounts of material. This system can be used to fabricate deposits similar but not identical to those prepared by means of conventional atmospheric plasma-spray systems based on gas-stabilized torches. As substrates flat carbon steel coupons (Euronorm S355) were used whereas the powder was fed in by compressed air through two injectors. Just before spraying, the steel was grit blasted with Al_2O_3 with a mean diameter of 650 μm. The deposited thickness was about 1.5 mm for self-supporting deposits. Thick deposits were stripped from the substrate by a releasing agent or by thermal cycling between +200 and -70°C.

For manufacturing of BT samples a Gas-Stabilized Plasma gun (GPS) was used to perform Atmospheric Plasma Spraying (APS) process. The conventional d.c. GPS gun F4 consisted of a thoriated tungsten cathode of 10 mm in diameter with a conical tip and a copper anode/nozzle. The plasma gas mixture used was argon/hydrogen with the total flow rate 60 slm. The powder was injected perpendicularly to the plasma jet axis with argon as a carrier gas (at constant flow rate 5 slm at pressure 0.3 MPa for all spray experiments) through an injector located 3 mm downstream (called external injection) of the torch nozzle exit. The system can process 1 to 5 kg/hour of a ceramic powder. Barium titanate was sprayed at arc power around 30 kW. Spray distance was 100 mm and plasma spraying deposition time about five minutes to reach the thickness 0.9 to 1 mm. Substrates, rectangular shaped (120x20 mm^2) 3 mm thick, were made of carbon steel (Euronorm S355). Just before spraying, they were grit blasted with Al_2O_3 with a mean diameter of 400 μm. The substrates were disposed on a rotating sample holder which diameter was 90 mm. This substrate holder was rotated (tangential speed of 1 m/s) with a horizontal axis and simultaneously translated back and forth orthogonally to the plasma jet axis at a velocity of 24 mm/sec, with an excursion of 160 mm, the plasma torch being stationary.

2.3 Characterization techniques

X-ray diffraction (XRD) was performed as a phase identification with SIEMENS D5000™ equipment *allowed* identifying *phases* present within powders and coatings. For estimation of the crystallinity of the plasma sprayed BT coating relative peak areas have been used. These have been calculated from relative ratios of the areas of the three main peaks (101, 111 and 200) from the tetragonal titanate phase.

Raman spectra were collected by the FORAM 685 apparatus which is equipped by a 685 nm laser with output power up to 40 mW. Spectral resolution 8 cm^{-1} and various integration times from 10 to 60 seconds were used. Raman spectroscopy of BT was performed using a Lambda Solutions P1 apparatus – laser wavelength 785 nm, objective 50 x, integration time 25 s.The surface of the coating was polished before the test.

Infrared reflective spectra of CT samples were measured by Bruker IFS 113v Fourier transform spectrometer.

Microwave microscope Agilent AFM 5400 was used for simultaneous monitoring of the surface profile by AFM and dielectric response on external field applied at resonant frequency (approx. 2.6 MHz). This relatively new technique - near-field scanning microwave microscopy (SMM) permits characterization of the effects of inhomogeneities and defects in crystals, films, and compacts on the local dielectric behavior. By moving the tip/cavity assembly over a surface, one can map the microwave cavity resonant frequency *fr* and quality factor *Q* as a function of position and generate images of the sample. In addition to qualitative images, the microscope can provide quantitative characterization of local dielectric properties [Cheng, 2003].

The complex dielectric permittivity of CT was studied in the 440 Hz – 1 MHz frequency range and 10–270K temperature interval using HP 4192A impedance analyzer with a Leybold He-flow cryostat (operating range 5–300 K). The impedance of the cylindrical sample with Au electrodes sputtered on the cylinder ends was recorded on cooling rate of 2 K/min.

All other electric measurements were performed at room temperature. The deposits were stripped of from the substrates. The surfaces were ground after spraying to eliminate surface roughness. A thin layer of aluminum as the electrode was sputtered in a reduced pressure on the ground surface [Ctibor, 2003]. A three-electrode system was used with a guarded electrode, whereas an unguarded electrode was sputtered on the entire surface of the sample opposite side. The electric field was applied parallel with the spraying direction (i.e., perpendicular to the substrate surface). Capacity was measured in the frequency range from 120 Hz to 1 MHz using the impedance analyzer 4284A (Agilent, CA, USA). Applied voltage was 1V AC whereas the stabilized electric source was equipped with a micrometric capacitor type 16451A (Agilent, CA, USA). Relative permittivity ε_r was calculated from measured capacities C_P and specimen dimensions (Eq. 1)

$$C_P = \varepsilon_0 \times \varepsilon_r \times 1/k \tag{1}$$

where $\varepsilon_0 = 8.854 \times 10^{-14}$ F cm^{-1}; 1/k [cm] is defined as the ratio between the guarded surface and the thickness of the sample [Morey, 2003].

This same arrangement and equipment was used for the loss factor measurement at the same frequencies as capacity.

Electric resistance was measured with a special resistivity adapter – Keithley model 6105. The electric field was applied from a regulated high-voltage source and the values read by a multi-purpose electrometer (617C, Keithley Instruments, USA). The magnitude of the applied voltage was 100±2V DC. Volume resistivity was calculated from the measured resistance and specimen dimensions. Typically 4 - 5 specimens were measured and the average calculated.

3. Results

3.1 Spectroscopic measurements

Figure 1 shows the Raman spectra of plasma sprayed CT in comparison with the sintered sample. SD means stand-off distance, in millimeters, of the as-sprayed samples and "an" denotes annealed samples. Annealing details are given elsewhere [Ctibor, 2003].

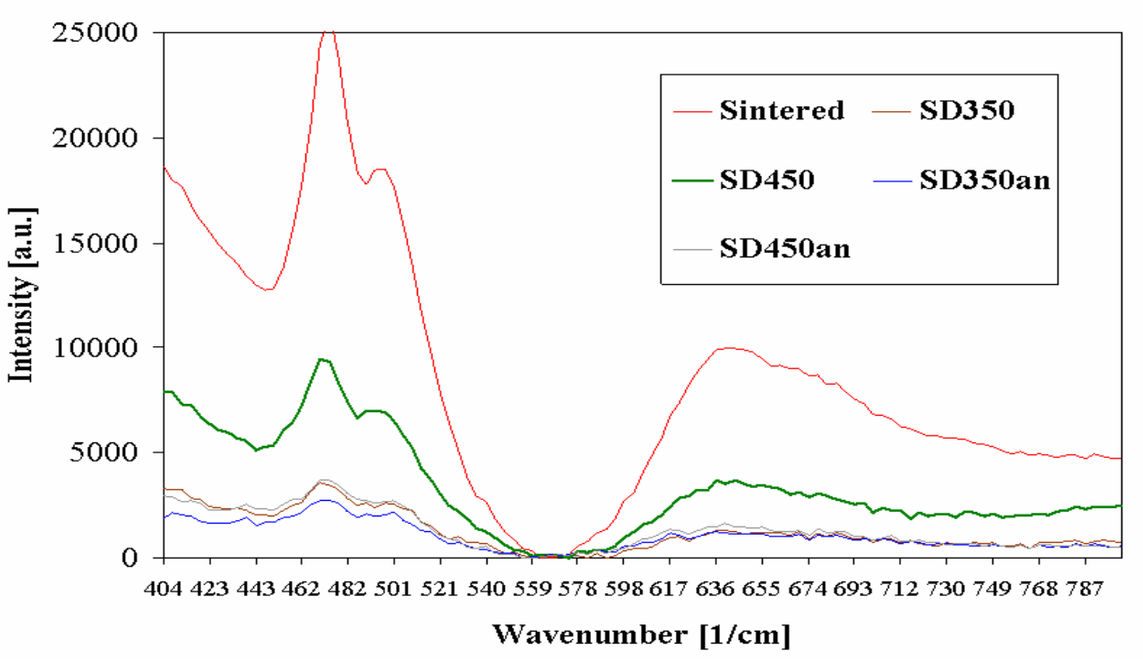

Fig. 1. Raman spectrum of $CaTiO_3$

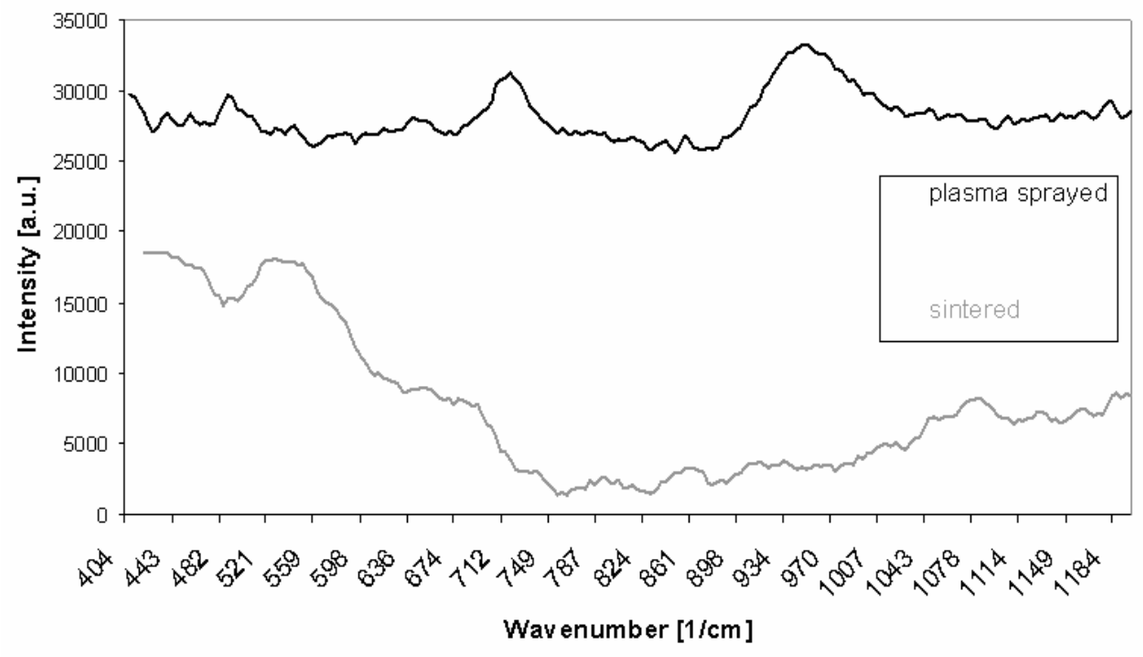

Fig. 2. Raman spectrum of $MgTiO_3$

The absolute values of the intensity of the reflection are associated with surface roughness and could be omitted. From the graph we see that the positions of all peaks are identical for all samples. Wavenumbers of all three main peaks observed at 471, 495, and 640 cm^{-1} are in

agreement with [Cavalcante, 2008]. The bands at 471 and 495 cm^{-1} are assigned to Ti–O torsional (bending or internal vibration of oxygen cage) modes [Hirata, 1996; Zheng, 2003]. The Ti–O stretching mode is centered at 640 cm^{-1} [Boutinaud, 2006]. Two small peaks at about 650 cm^{-1}, suggesting the simultaneous presence of [TiO_6] and [TiO_5] clusters, however in our case they are even less pronounced compare to [Cavalcante, 2008]. Also in our plasma sprayed samples incomplete organization of the $CaTiO_3$ lattice can be attributed to the defects in the covalent bond due to the oxygen vacancies ($VO\bullet\bullet$) between the clusters [TiO_6–$TiO_5 \cdot VO\bullet\bullet$] as in [Cavalcante, 2008]. This is associated with slightly reducing atmosphere in the plasma stream based on H and O atoms (water stabilization).
The Raman spectrum of MT is displayed on the **Fig. 2** in which the active modes at 478 cm^{-1} and 501 cm^{-1} [Hirata, 1996] are observed only on the coating. Next active modes are at 641 and 712 cm^{-1} [Hirata, 1996] and also were detected only on the coating, whereas in the sintered sample a shoulder centered at about 530 cm^{-1} is present.

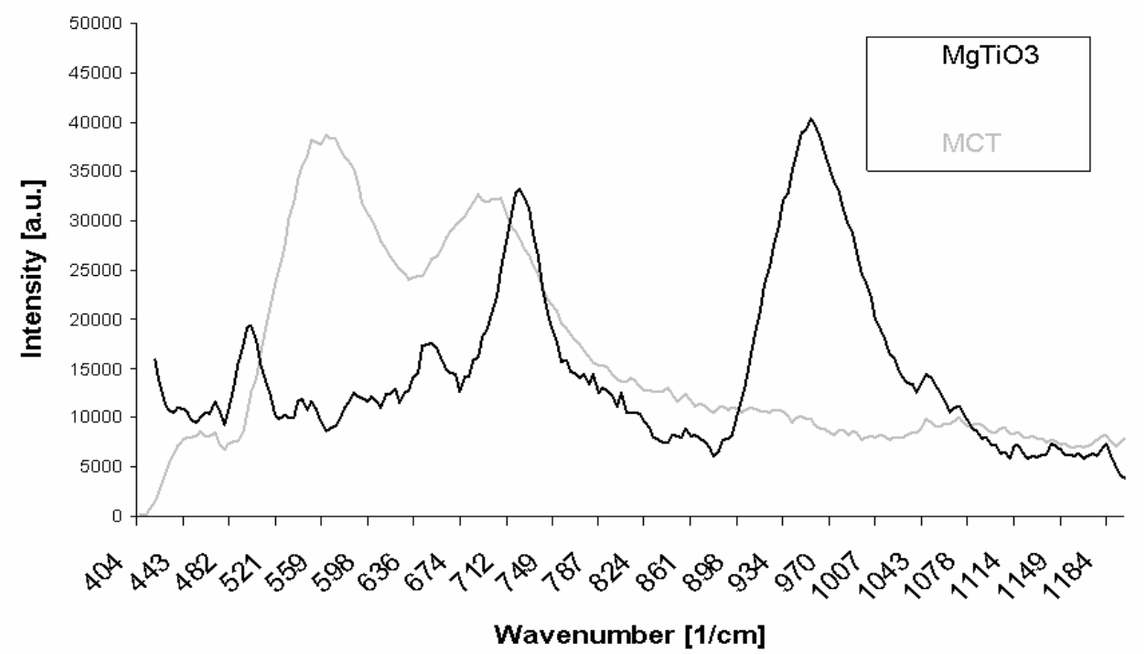

Fig. 3. Raman spectrum of MCT

The Raman spectrum of plasma sprayed MCT is displayed on the **Fig. 3** in comparison with MT measured at exactly the same conditions. We can see for MCT a red shift of the peak centered at 712 cm^{-1} in the case of MT. Other pronounced maximum is at 565 cm^{-1}. The Raman pattern of MCT is different compare to MT and CT and moreover it is not a simple combination of both of them. This is because of $MgTi_2O_5$ and Mg_2TiO_4 origin during the spraying, as confirmed by XRD [Ctibor, 2003]. However only two phases with different relative permittivity were detected by scanning microwave microscopy, see **Fig. 4**, similarly as in [Zhang, 2006]. Permittivities of $MgTi_2O_5$, Mg_2TiO_4 and MT are very similar together and very different from CT. **Figure 4** is a superposition of the AFM contact mode image (roughness) and scanning microwave microscopy capacitance mode image (colors). The image is artificially colored – blue and red zones represent different relative permittivity.

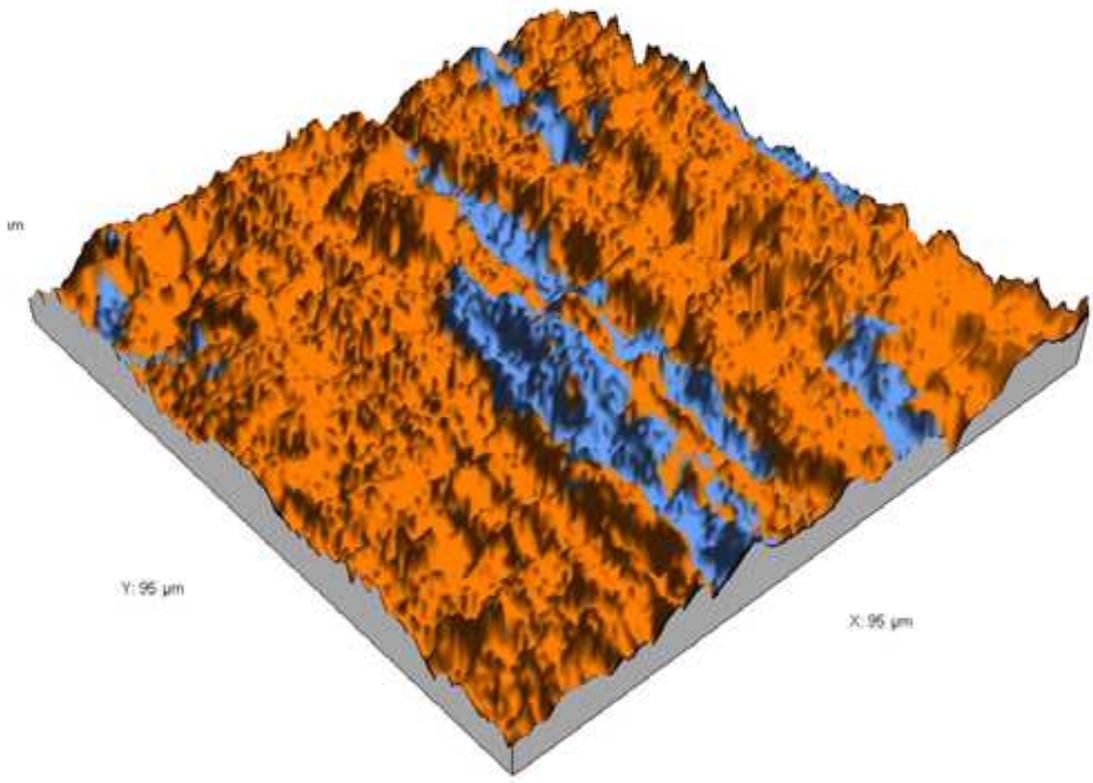

Fig. 4. Scanning microwave microscopy image of MCT as-sprayed surface (artificially colored – blue and red zones represent different relative permittivity)

CT (perovskite) is a high permittivity material $\varepsilon_r' = 170$ [Ferreira, 1997], $MgTiO_3$ (giekielite) has a low $\varepsilon_r' = 17$ [Zeng, 1997] and Mg_2TiO_4 (qandilite) also has even lower $\varepsilon_r' = 12$ [Haefie, 1992]. However SMM setup is not able to distinguish well the two last phases [Wing, 2006], also in our **Fig. 4** the blue lamellas correspond to CT, c.f. **Fig. 5**, and the red background to all other phases.

Raman spectrum of BT coating is displayed on **Fig. 6**. The spectrum with peaks at 311 and 507 cm^{-1} corresponds to tetragonal phase of $BaTiO_3$ [Souza, 2006]. At low oxygen pressure which is the condition relevant for plasma spraying, the density of oxygen vacancies is higher, and then the expansion of the lattice volume is greater [Souza, 2006]. This is why the Raman modes shift to lower frequencies: 507 cm^{-1} in our case instead of 518 cm^{-1} [26] or 532 cm^{-1} in [Souza, 2006] for the A_1 torsion mode. Raman spectrum of the long-SD coating is practically identical.

The modes further split into longitudinal (LO) and transverse (TO) components. The spectrum in **Fig. 6** shows the stretching mode of A1(TO_1), A1(TO_2) and A1(TO_3) at around 163, 259 and 507 cm^{-1}, respectively [Mattsson, 2010; Guo, 2005]. The stretching mode of E (TO_2) appeared at 311 cm^{-1}, while A1(LO_1) stretching modes at 188 cm^{-1} and A1(LO_2) at about 470 cm^{-1} [Mattsson, 2010], however the last one was not very pronounced in our case. By the Raman spectroscopy presence of TiO_2 in anatase form was mentioned - the peak at about 645 cm^{-1} was observed in TiO_2 film [Giolli, 2007] or coating [Buralcov, 2007]. Elsewhere [Ostapchuk, 2005] such a peak was shown without comments. In our case also week peak at 631 cm^{-1} was detected, which can correspond to anatase-TiO_2 individual phase in the $BaTiO_3$ coating.

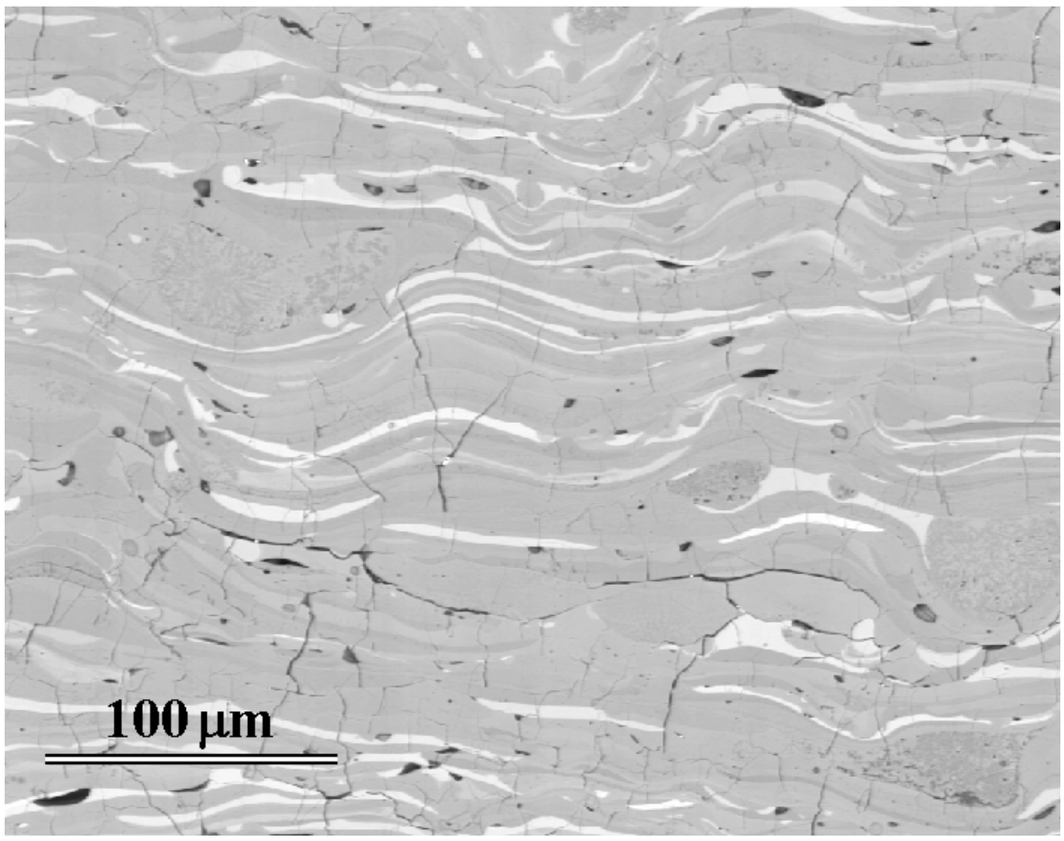

Fig. 5. SEM-BE image showing the lamellar microstructure

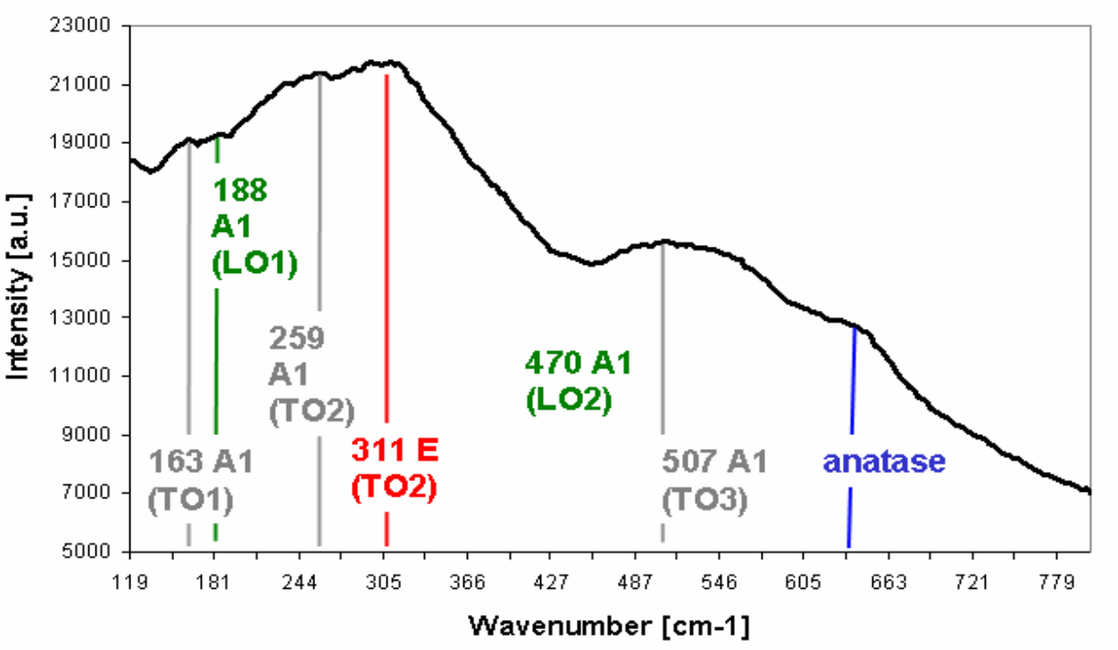

Fig. 6. Raman spectrum of plasma sprayed $BaTiO_3$

Figure 7 shows the infrared spectra of plasma sprayed CT in comparison with the sintered sample. The infrared-active mode at 575 cm^{-1}, assigned to the Ti–O stretch, and also the mode at 455 cm^{-1}, assigned to the Ti–O_3 torsion, are present in both samples with the same intensity. The slightly more pronounced local valley in the case of plasma sprayed sample – localized at about 680 cm^{-1} is the only subtle distinction.

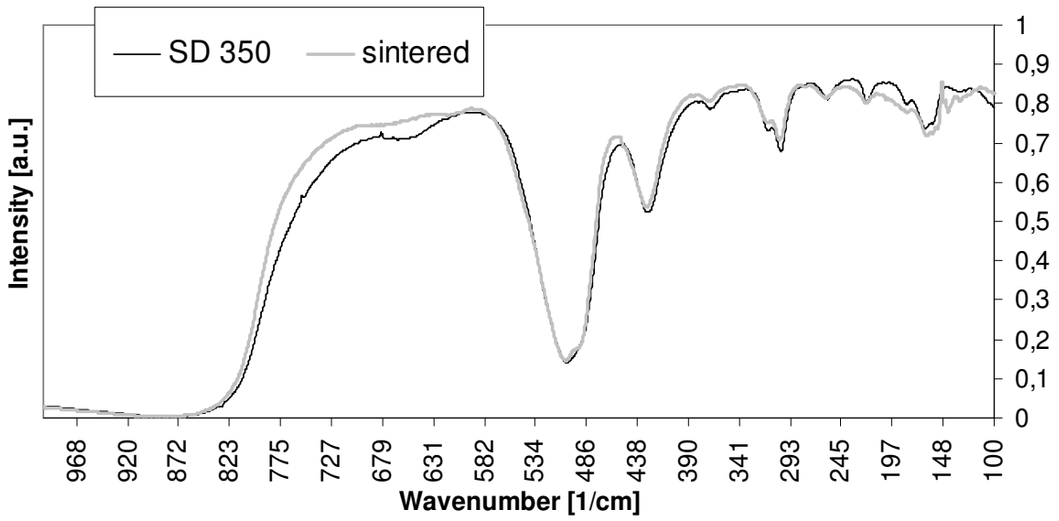

Fig. 7. Infrared spectrum of $CaTiO_3$

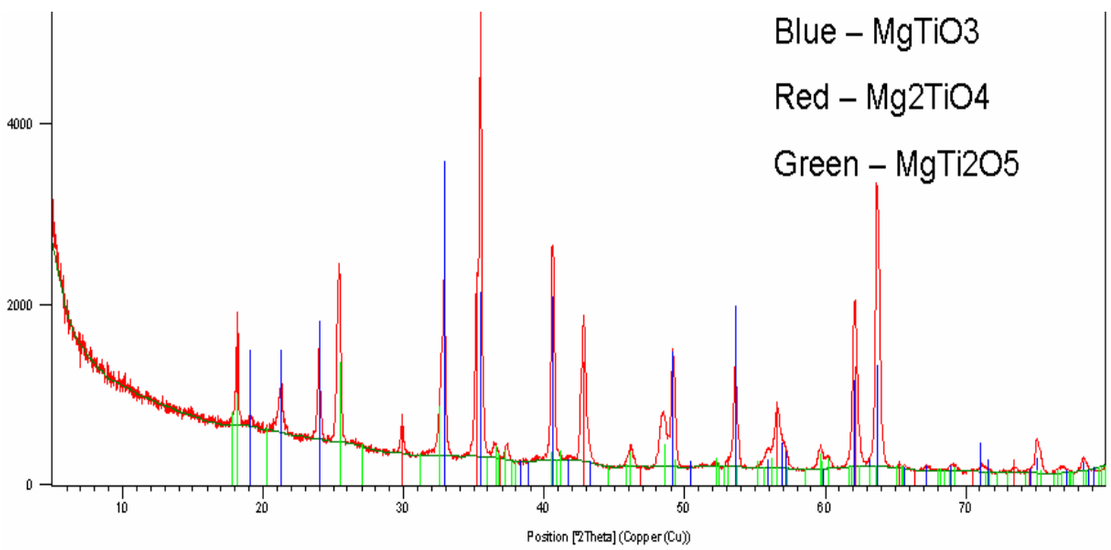

Fig. 8. XRD pattern of plasma sprayed $MgTiO_3$

According X-ray diffraction measurement of CT coating, the phase composition is the same as in the feedstock powder – pure $CaTiO_3$ (PDF2 card No. 00-022-0153). The XRD pattern of MT, **Fig. 8**, shows that the original metatitanate partly decomposed during the spray process on Mg_2TiO_4 and $MgTi_2O_5$. Al these components are present also in MCT coating, **Fig. 9**, whereas also $CaTiO_3$ is present as an individual phase.

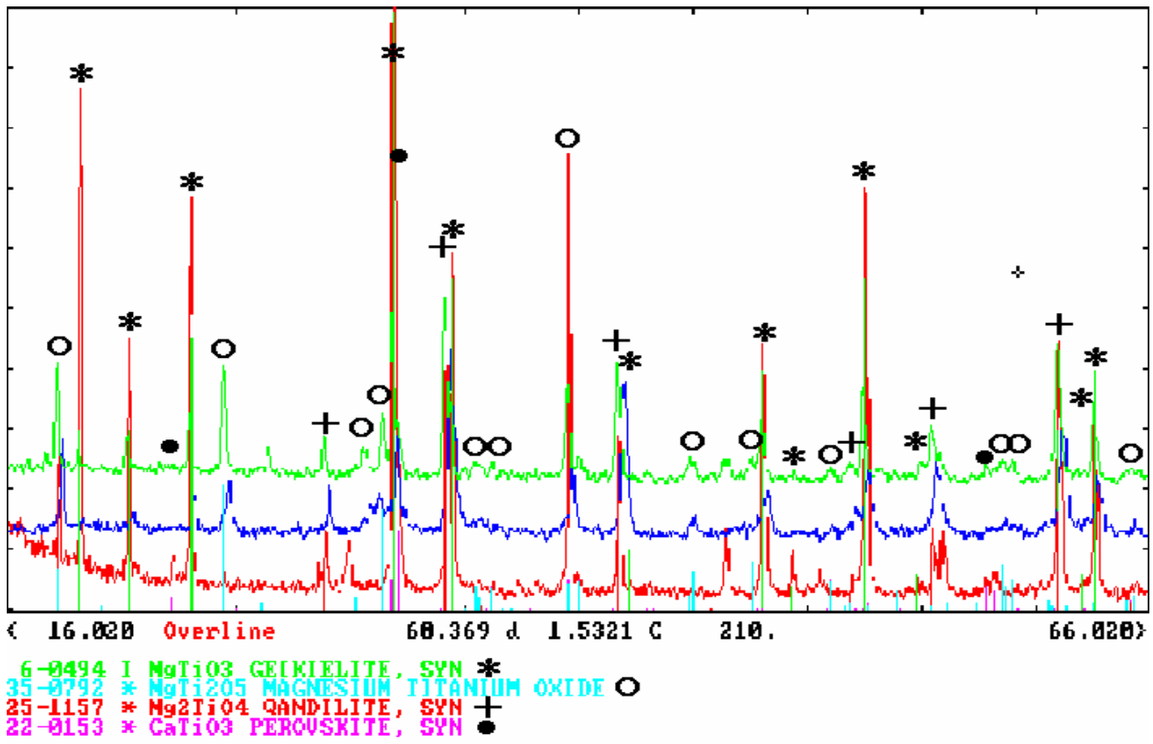

Fig. 9. XRD pattern of plasma sprayed MCT

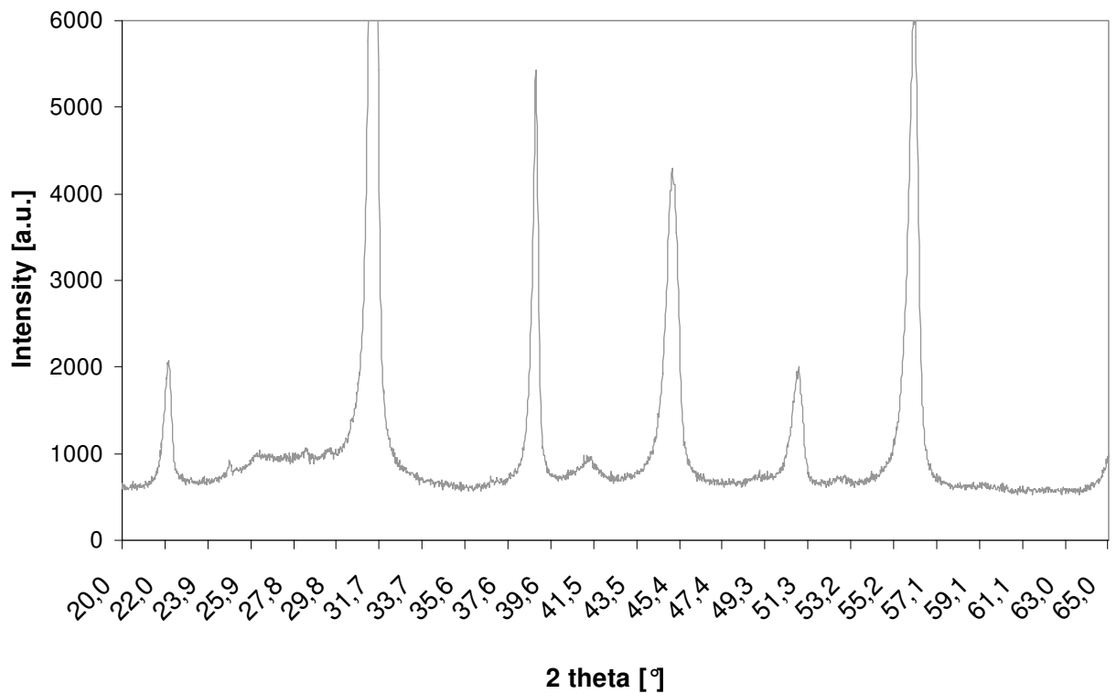

Fig. 10. XRD pattern of plasma sprayed BT coating

The XRD pattern of BT, **Fig. 10**, corresponds strictly to the tetragonal phase (PDF2 card No. 01-081-2204), which was confirmed to be the constituent of the feedstock powder as well as of the coatings. Intensity ratio of individual peaks of the feedstock as well as of the coatings is very similar to patterns reported in the literature [Wang, 2008]. In the coating, certain quantity of amorphous phase is present, manifested itself by a halo centered on 28° 2θ in the pattern, and quantified as 10 %.

3.2 Dielectric measurements

Dielectric properties of plasma sprayed $CaTiO_3$ between 10 K and room temperature are displayed on the **Figures 11 to 13**. The incipient ferroelectricity of CT [Lemanov, 1999; Sudheendran, 2008] is suppressed in the case of plasma sprayed coatings, see **Fig. 11**. Rather relaxor type of behavior takes place. Relaxor features are believed to be connected with a situation when more than one type of ions occupies equivalent crystallographic position. One of the most important features of relaxors is their low frequency dispersion at maximum dielectric permittivity. The other features of this include dependence of phase transition temperature on the method of its determination. The origin of such properties is probably connected with a presence of microscopic polar regions (nano-domains) in these materials [Bak, 2009]. With temperature falling down also the ε" values decrease to minimum (for a given frequency), cf. **Fig. 12**.

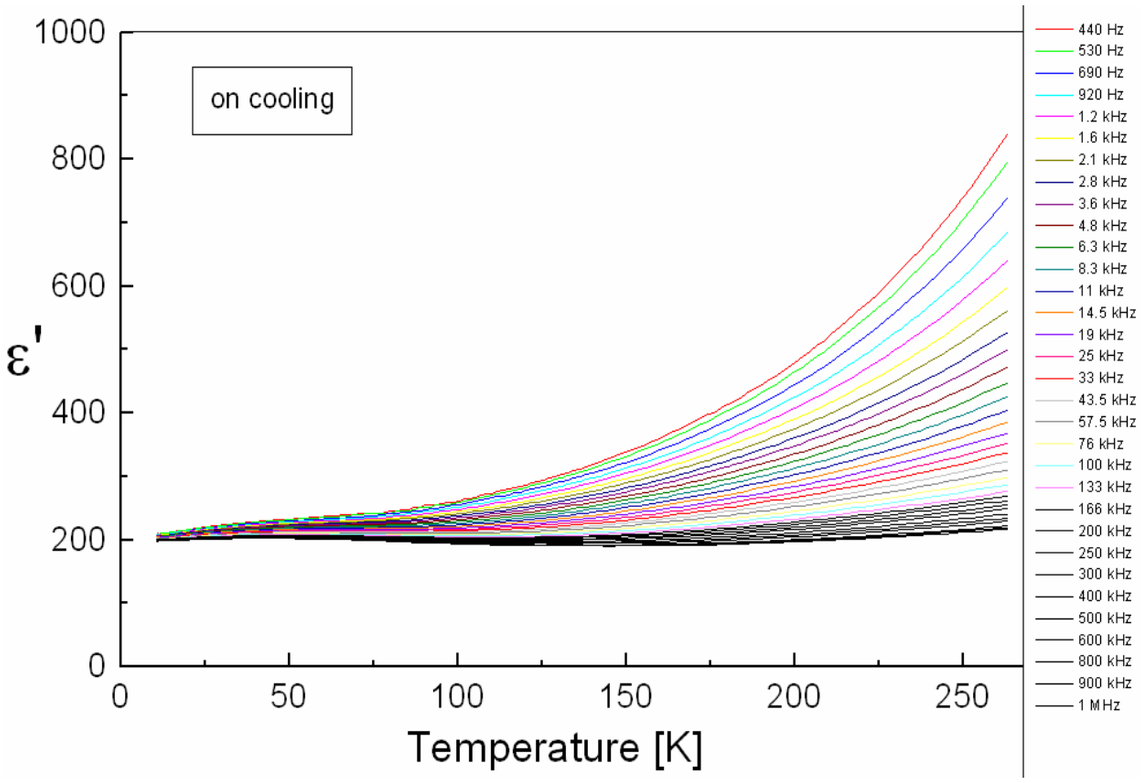

Fig. 11. Real part of permittivity of plasma sprayed $CaTiO_3$ between 10 K and room temperature

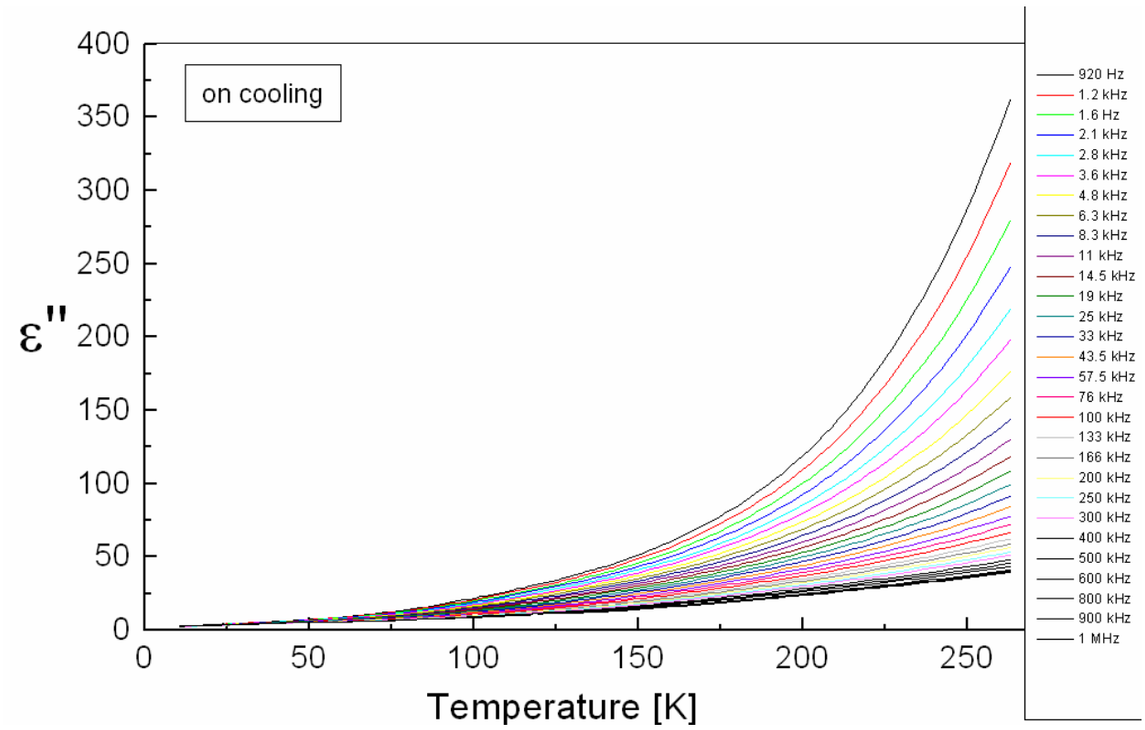

Fig. 12. Imaginary part of permittivity of plasma sprayed $CaTiO_3$ between 10 K and room temperature

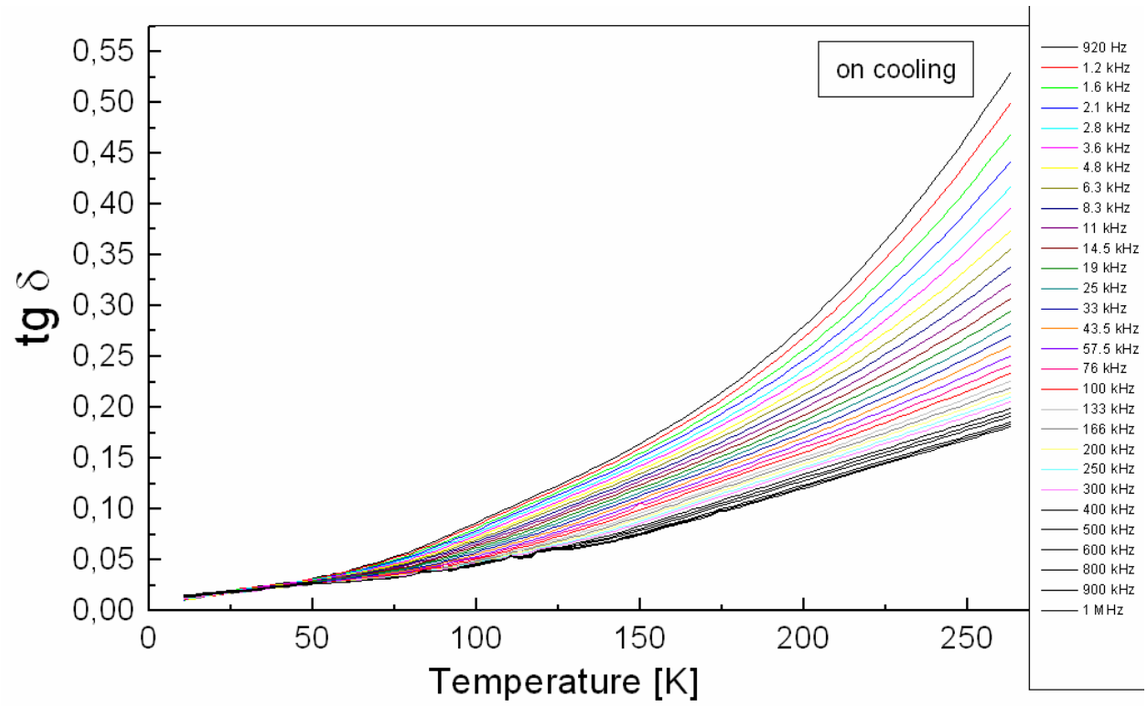

Fig. 13. Loss tangent of plasma sprayed $CaTiO_3$ between 10 K and room temperature

In the studied frequency range, the relative permittivity of all specimens exhibits significant ionic relaxation process [Dervos, 2004]. Strong relaxation effects is shown by the ε_r' reduction with the operating frequency, see **Fig. 14**. In Ti-based materials, the concentrations of intrinsic defects are determined by oxygen partial pressure and, additionally, variations in defect concentrations can be detected by conductivity measurements. At low oxygen partial pressures the materials show n-type conduction with oxygen vacancy as the dominant defect while at high oxygen partial pressures the materials show p-type conduction with the cation vacancy as the dominant defect. For the different materials the transition from n-type conduction to p-type conduction occurs at different oxygen partial pressures [Hu, 2011]. The partial pressure of oxygen required to reduce for example TiO_2 to Ti_2O_3, Ti_3O_5 or Ti_4O_7 is of the order of 10^{-5} Pa at around 2000°C, while during plasma spraying in the air, oxygen partial pressure does not go below 1 Pa [Ctibor, 2010]. Dielectric losses of our titanate samples, namely BT and CT are however high, see **Fig. 15**. Electric conductivity is responsible for it with dominating contribution of dc-conductivity component. The ε'' dependence can be treated as typical for materials with dc-conductivity which dominates over relaxation processes [Bak, 2008].

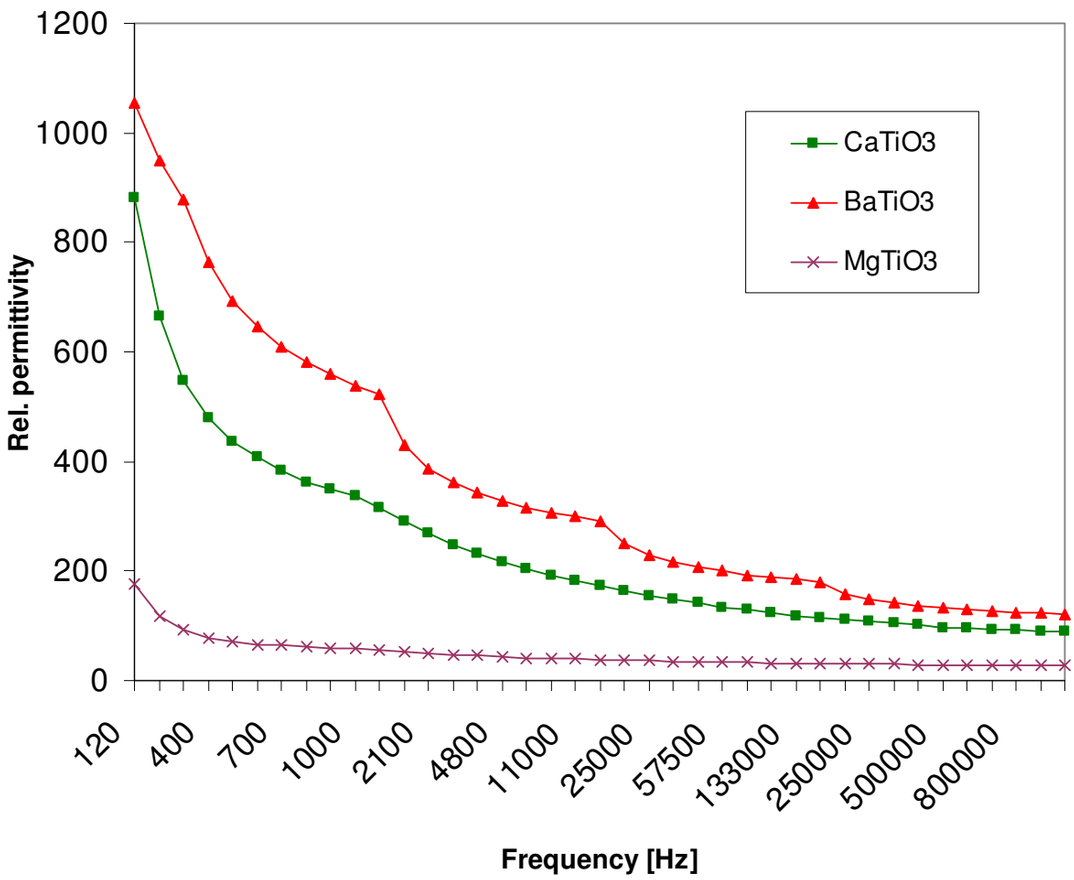

Fig. 14. Frequency dependence of the relative permittivity of plasma sprayed $BaTiO_3$, $CaTiO_3$, and $MgTiO_3$ at room temperature

Table 1 shows the volume resistivity and **Fig. 16** corresponding conductivity of plasma sprayed and sintered BT, CT, MT and MCT materials. We see the different values with typically several orders of magnitude lower resistivity values for plasma sprayed specimen compare to sintered materials.

Sample	BT (P)	BT (S)	CT (P)	CT (S)	MT (P)	MT (S)	MCT (P)	MCT (S)
ρ [Ωm]	6.08×10^{4}	2.42×10^{9}	7.51×10^{9}	1.41×10^{12}	1.15×10^{8}	6.90×10^{11}	1.17×10^{7}	7.54×10^{11}

Table 1. Volume resistivity of studied materials (P – plasma sprayed, S – sintered)

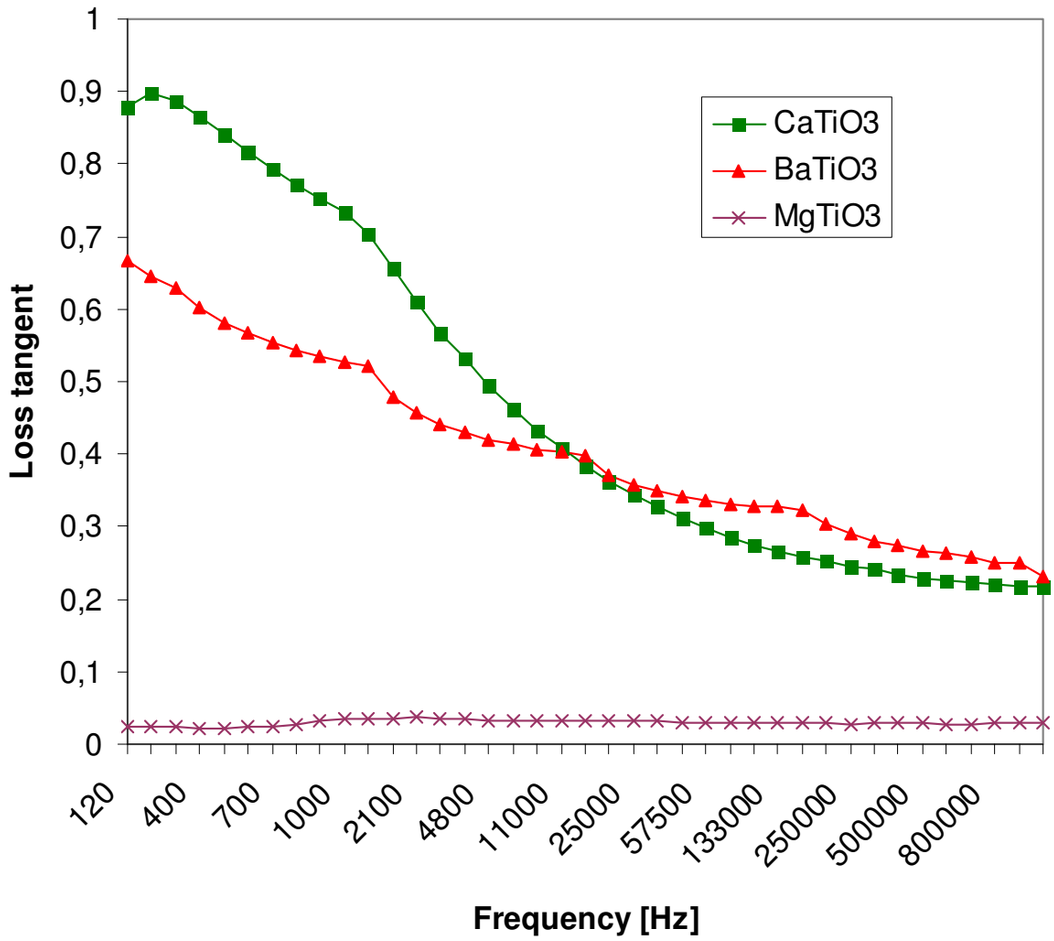

Fig. 15. Frequency dependence of the loss tangent of plasma sprayed $BaTiO_3$, $CaTiO_3$, and $MgTiO_3$ at room temperature

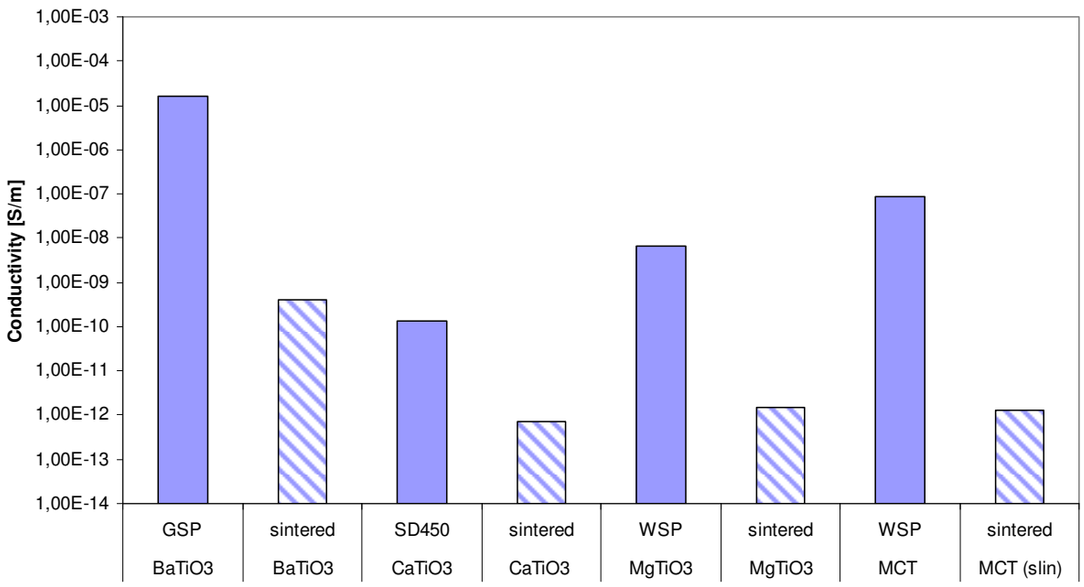

Fig. 16. Conductivity of plasma sprayed and sintered BT, CT, MT and MCT

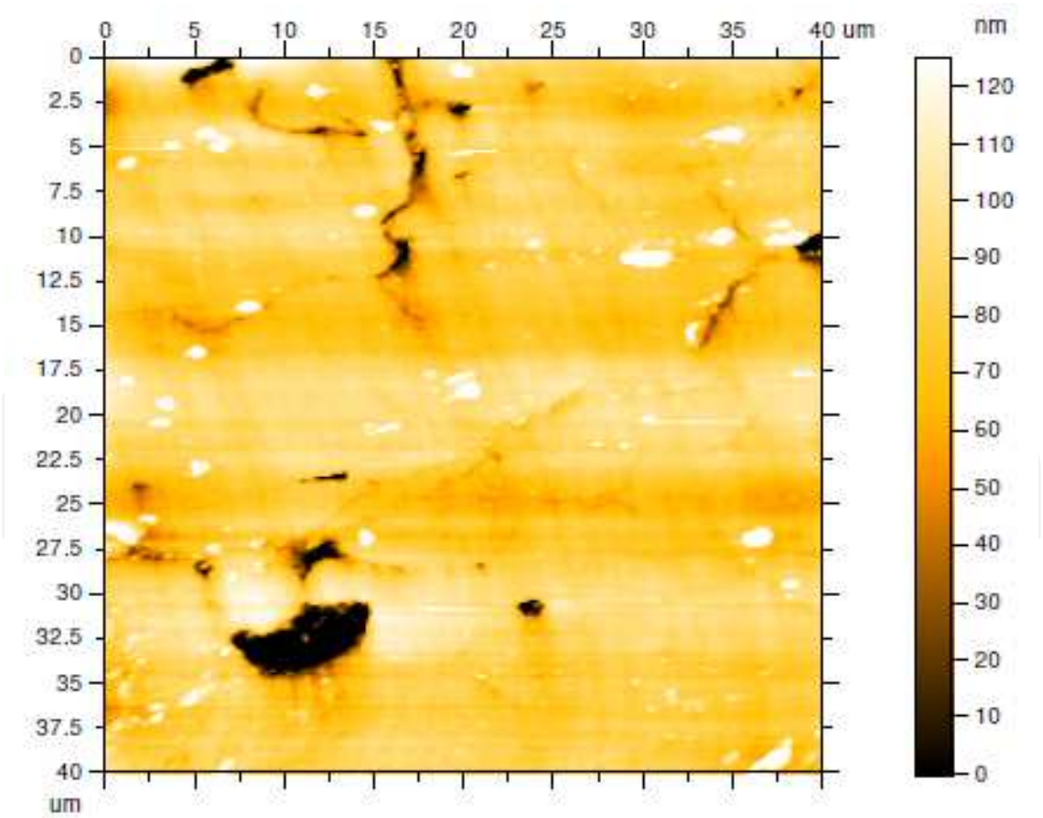

Fig. 17. AFM contact mode image of $BaTiO_3$ (in plane orientation). Roughness representation: peaks are lighter and valleys darker (black color represents pores)

3.3 Scanning microwave microscopy

Scanning microwave microscopy images of BT are given on **Figs. 17** and **18**. AFM images represent surface roughness. Since the surface was materialographically polished, the subtle differences in the roughness are associated with hardness of various phases. These phases are concentrated predominantly in individual lamellas, cf. MCT SEM micrograph in the **Fig. 5**. In the case of BT, the difference between lamellas is mainly in terms of Ba/Ti ratio [Ctibor 2, 2010]. Such a feature is, as expectable, more easily visible on cross sections, **Fig. 19,** then on in-plane (i.e. spray direction) sections **Fig. 18.** The lamellas, red and yellow on capacitance mode images, are more Ti-rich (higher permittivity) whereas blue areas are Ba-rich (lower permittivity). The Ba-rich phase has slightly lower hardness (hardness measured by us: $BaTiO_3$ is about 6.5 GPa versus TiO_2 about 11.0 GPa; BaO not reported as a layer). The Ba-rich phase is darker on AFM contact mode image, since it is more easily worn-out by polishing process. These "steps" on border of lamellas are about 80 nm high, see also **Fig. 20**, which height is consistent with observations made by SEM.

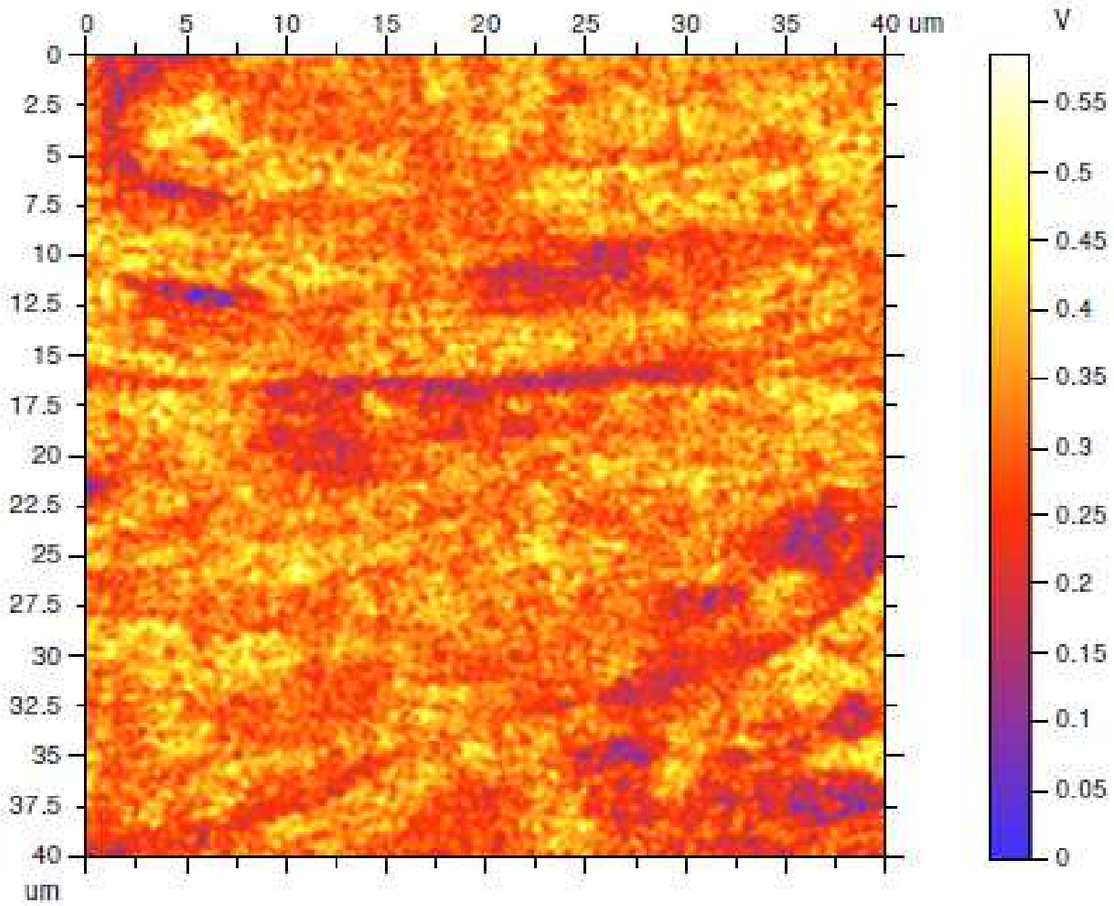

Fig. 18. Scanning microwave microscopy image of $BaTiO_3$ (in plane orientation) - artificially colored: blue and red zones represent different relative permittivity

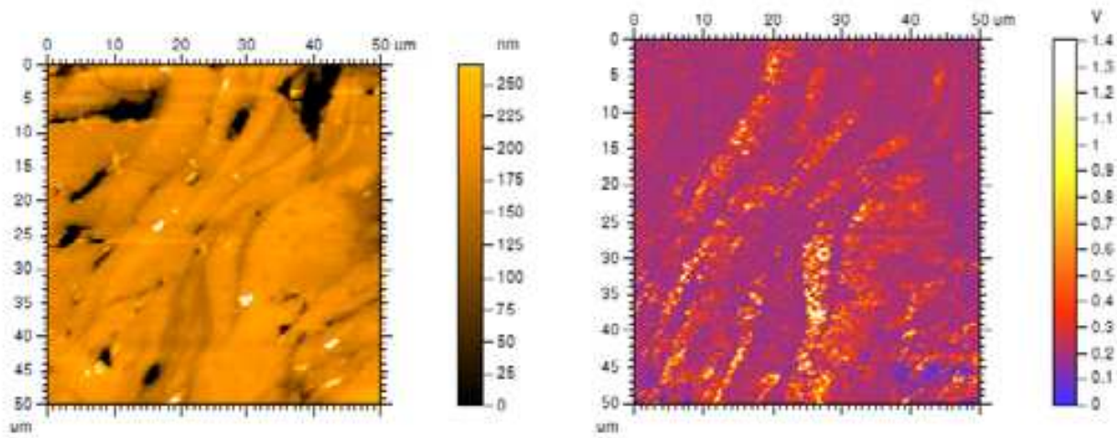

Fig. 19. AFM contact mode image of $BaTiO_3$ (cross sectional orientation). Left: Roughness representation: peaks are lighter and valleys darker (black color represents pores). Right: Scanning microwave microscopy image of $BaTiO_3$ (cross sectional orientation) - artificially colored: blue and red zones represent different relative permittivity

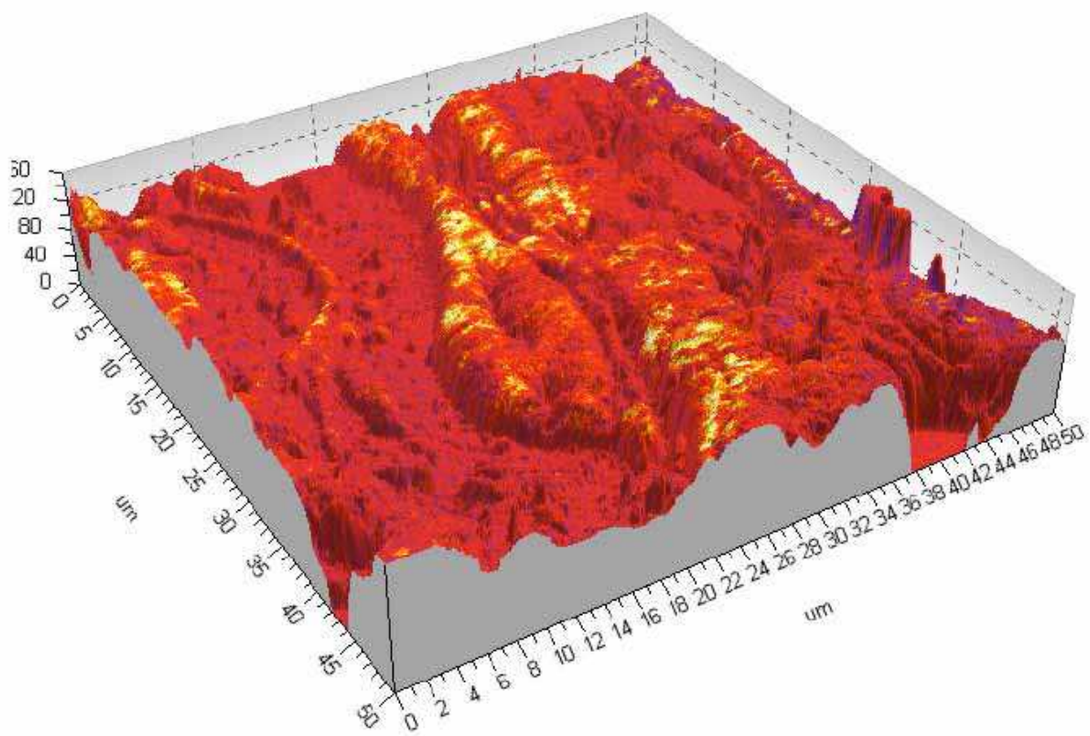

Fig. 20. Superposition of the AFM contact mode image and SMM image - BaTiO3 cross section. Hard and high-permittivity Ti-rich lamellas are yellow

4. Conclusions

$BaTiO_3$, $CaTiO_3$, $MgTiO_3$ and a mixture of the last two materials with 5 wt.% of $CaTiO_3$ in $MgTiO_3$ were plasma sprayed by two complementary spray techniques. Raman and infrared

spectroscopic measurements were carried out on plasma sprayed titanates. Coating samples were tested as mono-block capacitors. Volume dc-resistivities of the materials were summarized. Microwave microscopy was used for mapping of the dielectric response of selected samples.

$CaTiO_3$ exhibits anomalous dielectric losses because of intrinsic conductivity. Relaxor type of behavior takes place at dielectric measurements, whereas dc-conductivity is responsible for the high dielectric losses. All coatings are slightly oxygen deficient – however under detection limits of XRD materials – the color of all of them is darker compare to sintered samples.

Polarization of grain boundaries combined with n-type conduction with oxygen vacancy as the dominant defect contributes to the observed pseudo-relaxor response of $BaTiO_3$ and $CaTiO_3$ to AC electric field. $MgTiO_3$ as a low-loss material has the above mentioned effects slightly suppressed and is more similar to sintered bulk. The existence of irregularities in the crystal lattice was confirmed by spectroscopic measurements. Plasma spraying of applicable ceramic dielectrics able to substitute bulk parts will need further research. In the other hand, plasma spraying, with its possibility to cover wide range of substrate materials with thick coatings having very versatile thicknesses and areas, offers promising way to future development.

5. Acknowledgment

The authors thank to J. Dubsky (IPP ASCR) for XRD measurements, to M. Savinov (Inst. of Physics, ASCR) for the temperature measurement of dielectric properties of $CaTiO_3$ and to V. Zelezny (Inst. of Physics, ASCR) for doing the infrared spectroscopy. Scanning microwave microscopy was done by M. Fenner (Agilent, Germany). The company ELMES, Lt.D. is acknowledged for lending of the Foram device. $BaTiO_3$ was sprayed at University of Limoges, France.

This work was supported by IPP ASCR under project AV0Z20430508.

6. References

Bak W.; Starzyk, F.; Kajtoch, C. & Nogas-Cwikiel, E (2008). Elevated temperature induced dispersion phenomena in $Ba_{1-x}Na_xTi_{1-x}Nb_xO_3$. *Archives of Materials Science and Engineering*, Vol. 29, No. 1, pp. 5-9

Bak W. (2009). Study of the relaxor behaviour in $Ba_{0.68}Na_{0.32}Ti_{0.68}Nb_{0.32}O_3$ ceramic. *Journal of Achievements in Materials and Manufacturing Engineering*, Vol. 37, pp. 24-27

Boutinaud, P.; Tomasella, E.; Ennajdaoui A. & Mahiou R. (2006), Structural characterization and luminescent properties of $CaTiO_3:Pr^{3+}$ thin films deposited by radio frequency sputtering.*Thin Solid Films*, Vol. 515, pp. 2316–2321

Buchanan, R.C. (2004). Ceramic materials for electronics (3rd edition), M. Dekker, New York

Burlacov, I.; Jirkovsky, J.; Kavan, L.; Ballhorn, R. & Heimann, R.B. (2007). Cold gas dynamic spraying (CGDS) of TiO_2 (anatase) powders onto poly(sulfone) substrates: Microstructural characterisation and photocatalytic efficiency, *Journal of Photochemistry and Photobiology A: Chemistry*, Vol. 187, pp. 285–292

Cavalcante, L.S. et al. (2008). Synthesis, structural refinement and optical behavior of $CaTiO_3$ powders: A comparative study of processing in different furnaces. Chemical *Engineering Journal*, Vol. 143, pp. 299–307

Ctibor, P.; Sedlacek, J.; Neufuss, K. & Chraska, P. (2003). Dielectric relaxation in calcium titanate-containing ceramics prepared by plasma spraying. *Ceramics International*, Vol. 29, pp. 955-960

Ctibor, P. & Hrabovsky, M. (2010). Plasma sprayed TiO_2: The influence of power of an electric supply on particle parameters in the flight and character of sprayed coating. Journal of the European *Ceramic Society*, Vol. 30, pp. 3131-3136

Ctibor, P.; Ageorges, H.; Sedlacek, J. & Ctvrtlik, R. (2010). Structure and properties of plasma sprayed $BaTiO_3$ coatings, *Ceramics International*, Vol. 36, pp. 2155-2162

Cheng H.-F. et al. (2003). Study of second-phases in $Ba(Mg_{1/3}Ta_{2/3})O_3$ materials by microwave near-field microscopy. *Journal of the European Ceramic Society*, Vol. 23, pp. 2667–2670.

Dent, A.H. et al. (2001). High velocity oxy-fuel and plasma deposition of $BaTiO_3$ and $(Ba,Sr)TiO_3$. Materials Science and Engineering B, Vol. 87, pp. 23-30.

Dervos, C.T.; Thirios, E.; Novacovich, J.; Vassiliou, P. & Skafidas, P. (2004). Permittivity properties of thermally treated TiO_2. *Materials Letters*, Vol. 58, pp. 1502– 1507

Ferreira, V. M.; Azough, F.; Freer R. & Baptista J. L. (1997). The Effect of Cr and La on MgTiO3 and MgTiO3–CaTiO3 Microwave Dielectric Ceramics, *Journal of Materials Research*, Vol. 12, pp. 3293–3299

Giolli C. et al. (2007). Characterization of TiO_2 coatings prepared by a modified electric arc-physical vapour deposition system. *Surface & Coatings Technology*, Vol. 202, pp. 13–22

Guo H.Z. et al. (2005). Structure dynamics of strongly reduced epitaxial $BaTiO_{3-x}$ studied by Raman scattering. *Journal of the European Ceramic Society*, Vol. 25, pp. 2347-2352.

Haefie H. et al. (1992). Mg2TiO4 as a novel substrate for high-temperature superconducting thin films, *Applied Physics Letters*, Vol. 61, pp. 9-19

Hu P. et al. (2011). Influence of thermal treatments on the low frequency conductivity and microwave dielectric loss of $CaTiO_3$ ceramics, *Materials Science and Engineering* B, Vol. 176, No. 5, pp. 401-405.

Huang, C.-L.; Pan, C.-L. & Shium S.-J. (2002). Liquid phase sintering of $MgTiO_3$-$CaTiO_3$ microwave dielectric ceramics.

Materials Chemistry and Physics, Vol. 78, pp. 111–115

Hirata, T.; Ishioka K. & Kitajima M. (1996). *Journal of solid state chemistry*, Vol. 124, pp. 353–359

Jiang, Y.; Guo, R. & Bhalla, A. S. (1998). LHPG grown crystal fibers of $MgTiO_3$-$CaTiO_3$ eutectic system. *Journal of Physics and Chemistry of Solids*, Vol. 59, pp. 611-615

Jin, H.Z. et al. (2003). An interfacial defect layer observed at $(Ba,Sr)TiO_3$-Pt interface. *Thin Solid Films*, Vol. 429, pp. 282-285.

Lemanov, V.V.; Sotnikov, A.V.; Smirnova, E.P.; Weihnacht, M. & Kunze, R. (1999). Perovskite $CaTiO_3$ as an incipient ferroelectric, *Solid State Communications*, Vol. 110, pp. 611–614

Mattsson A. & Oesterlund L. (2010). Adsorption and photoinduced decomposition of acetone and acetic acid on anatase, brookite, and rutile TiO_2 nanoparticles, *Journal of Physical Chemistry*, Vol. 114 C, pp.14121–14132

Mitic, V.V. & Mitrovic I. (2001). The influence of Nb_2O_5 on $BaTiO_3$ ceramics dielectric properties, *Journal of the European Ceramic Society*, Vol. 21, pp. 2693-2696

Morey, O.; Goeuriot P.; Juve D. & Treheux D. (2003). Dielectric investigations on 'MgAlON' compounds: Role of nitrogen content. *Journal of the European Ceramic Society*, Vol. 23 pp. 345-350.

Ostapchuk T. et al. (2005). Soft-mode spectroscopy of $BaTiO_3$ thin films. *Journal of the European Ceramic Society*, Vol. 25, pp. 3063–3067

Setter, N. & Waser, R. (2000). Electroceramic materials, *Acta Materialia*, Vol. 48, pp.151-178

Simon-Seveyrat, L.; Hajjaji, A.; Emziane, Y.; Guiffard, B. & Guyomar, D. (2007). Re-investigation of synthesis of $BaTiO_3$ by conventional solid-state reaction and oxalate coprecipitation route for piezoelectric applications, *Ceramics International*, Vol. 33, pp. 35-40

Souza I.A. et al. (2006). Theoretical and experimental study of disordered $Ba_{0.4}$ $Sr_{0.55}TiO_3$ photoluminescence at room temperature, *Chemical Physics*, Vol. 322, pp. 343–348

Sudheendran, K. & James Raju K.C. (2008). Temperature dependent impedance and dielectric properties of $0.7CaTiO_3$–$0.3NdAlO_3$ ceramics. *Indian journal of engineering & material sciences*,Vol. 15, p. 133-136

Waser, R. (1999). Modeling of Electroceramics - Applications and Prospects, *Journal of the European Ceramic Society*, Vol. 19, pp. 655-664

Wang, X.; Zhang, L.; Liu, H.; Zhai J. & Yao X. (2008). Dielectric nonlinear properties of $BaTiO_3$–$CaTiO_3$–$SrTiO_3$ ceramics near the solubility limit, *Materials Chemistry and Physics*, Vol. 112, pp. 675-678

Wing, Z. N.; Halloran J. W.; Zhang, Q.; McGinn, P. J. (2006). Variable Dielectrics in the Calcium Magnesium Titanate System Characterized with Scanning Microwave Microscopy, *Journal of the American Ceramic Society*, Vol. 89, No. 5, pp. 1610–1614

Wu, L. et al. (2009). Dielectric properties of barium titanate ceramics with different materials powder size, *Ceramics International*, Vol. 35, pp. 957-960

Yu, P.; Cui, B. & Chany, Z. (2009). Preparation and characterization of Ag-doped $BaTiO_3$ based X7R ceramics, *Materials Research Bulletin*, Vol. 44 , pp. 893-897

Zeng, J.; Wang, H.; Shang, S.; Wang, Z. & C. Lin (1997). Preparation of Textured Mg_2TiO_4 Thin Films on Si Substrate by Atmospheric Pressure Metallorganic Chemical Vapour Deposition, *J. Mater. Sci. Mater. Electron*., Vol. 8, pp. 159–162

Zhao, M.H.; Bonnell, D.A. & Vohs, J.M. (2008). Effect of ferroelectric polarization on the adsorption and reaction of ethanol on $BaTiO_3$, *Surface Science*,Vol. 602, pp. 2849-2855

Zhang Q. & McGinn P. J. (2006). Characterization of Calcium Titanate–Magnesium Titanate Eutectic by Scanning Microwave Microscopy, J*ournal of the American Ceramic Society*, Vol. 89, pp. 3817 – 3823

Zheng,H. et al. (2003). Raman spectroscopy of B-site order-disorder in $CaTiO_3$-based microwave ceramics. *Journal of the European Ceramic Society*, Vol. 23, pp. 2653–2659

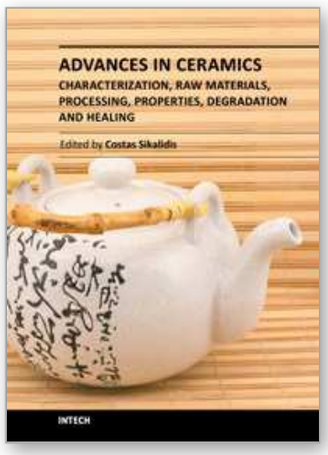

Advances in Ceramics - Characterization, Raw Materials, Processing, Properties, Degradation and Healing
Edited by Prof. Costas Sikalidis

ISBN 978-953-307-504-4
Hard cover, 370 pages
Publisher InTech
Published online 01, August, 2011
Published in print edition August, 2011

The current book consists of eighteen chapters divided into three sections. Section I includes nine topics in characterization techniques and evaluation of advanced ceramics dealing with newly developed photothermal, ultrasonic and ion spattering techniques, the neutron irradiation and the properties of ceramics, the existence of a polytypic multi-structured boron carbide, the oxygen isotope exchange between gases and nanoscale oxides and the evaluation of perovskite structures ceramics for sensors and ultrasonic applications. Section II includes six topics in raw materials, processes and mechanical and other properties of conventional and advanced ceramic materials, dealing with the evaluation of local raw materials and various types and forms of wastes for ceramics production, the effect of production parameters on ceramic properties, the evaluation of dental ceramics through application parameters and the reinforcement of ceramics by fibers. Section III, includes three topics in degradation, aging and healing of ceramic materials, dealing with the effect of granite waste addition on artificial and natural degradation bricks, the effect of aging, micro-voids, and self-healing on mechanical properties of glass ceramics and the crack-healing ability of structural ceramics.

How to reference
In order to correctly reference this scholarly work, feel free to copy and paste the following:

Pavel Ctibor and Josef Sedlacek (2011). Spectroscopic and Dielectric Characterization of Plasma Sprayed Titanates, Advances in Ceramics - Characterization, Raw Materials, Processing, Properties, Degradation and Healing, Prof. Costas Sikalidis (Ed.), ISBN: 978-953-307-504-4, InTech, Available from: http://www.intechopen.com/books/advances-in-ceramics-characterization-raw-materials-processing-properties-degradation-and-healing/spectroscopic-and-dielectric-characterization-of-plasma-sprayed-titanates

INTECH
open science | open minds

InTech Europe
University Campus STeP Ri
Slavka Krautzeka 83/A
51000 Rijeka, Croatia
Phone: +385 (51) 770 447
Fax: +385 (51) 686 166
www.intechopen.com

InTech China
Unit 405, Office Block, Hotel Equatorial Shanghai
No.65, Yan An Road (West), Shanghai, 200040, China
中国上海市延安西路65号上海国际贵都大饭店办公楼405单元
Phone: +86-21-62489820
Fax: +86-21-62489821

IntechOpen